Deeply bound K^-pp state in the ^{3}He(in-flight K^-,n) spectrum, and its moving pole near the $\pi\Sigma N$ threshold

Takahisa Koike[1,*] and Toru Harada[2,†]

[1]*Advanced Meson Science Laboratory, RIKEN Nishina Center, Wako-shi, Saitama 351-0198, Japan*

[2]*Research Center for Physics and Mathematics, Osaka Electro-Communication University, Neyagawa, Osaka, 572-8530, Japan*

(Received 24 August 2009; published 30 November 2009)

The formation of a deeply bound K^-pp state with $I = 1/2$, $J^\pi = 0^-$, by the ^{3}He(in-flight K^-,n) reaction is theoretically investigated in a distorted-wave impulse approximation using the Green's function method. The expected inclusive and semiexclusive spectra at $p_{K^-} = 1.0\,\mathrm{GeV}/c$ and $\theta_{\mathrm{lab}} = 0^\circ$ are calculated for the forthcoming J-PARC E15 experiment. We demonstrate these spectra with several phenomenological K^--"pp" optical potentials $U^{\mathrm{opt}}(E)$ that have an energy-dependent imaginary part multiplied by a phase space suppression factor, fitting to recent theoretical predictions or experimental candidates of the K^-pp bound state. The results show that a cusplike peak at the $\pi\Sigma N$ threshold is a unique signal for the K^-pp bound state in the spectrum including the $[K^-pp] \to Y + N$ decay process from two-nucleon K^- absorption, as well as a distinct peak of the K^-pp bound state. The shape of the spectrum is explained by the trajectory of a moving pole of the K^-pp bound state in the complex energy plane. The importance of the $[K^-pp] \to Y + N$ spectrum to extract clear evidence of the K^-pp bound state is emphasized.

DOI: 10.1103/PhysRevC.80.055208 PACS number(s): 25.80.Nv, 13.75.Jz, 36.10.Gv, 21.45.−v

I. INTRODUCTION

The antikaon-nucleon ($\bar{K}N$) interaction in nuclei is very important to elucidate the nature of high density nuclear matter [1]. Because the $\bar{K}NI = 0$ interaction is believed to be strongly attractive, one would expect the existence of deeply bound $\bar{K}$ nuclear states [2]. In particular, a three-body $\bar{K}NN$ (unstable) bound state with a $[\bar{K} \otimes \{NN\}_{I=1}]_{I=1/2}$, $J^\pi = 0^-$, configuration, which is called "K^-pp" here, is suggested to be the lightest and most fundamental $\bar{K}$ nucleus.

In 1963, Nogami [3] first discussed the possible existence of the K^-pp bound state using a rather crude calculation. About 40 years later, Yamazaki and Akaishi [4] resumed the study of the structure of the K^-pp bound state based on a quantitative few-body calculation with a phenomenological $\bar{K}N$ interaction that reproduces the mass and width of $\Lambda(1405)$ as a $\bar{K}$-N quasibound state. They predicted that the binding energy and width for the K^-pp state are B.E. = 48 MeV and Γ = 61 MeV, respectively. Many other theoretical works [5–12] have also supported the existence of the K^-pp bound state, but the predicted binding energies and widths do not converge (see Fig. 2). Shevchenko, Gal, and Mareš [5] performed a $\bar{K}NN$-$\pi\Sigma N$ coupled-channel Faddeev calculation using phenomenological $\bar{K}N$-$\pi\Sigma$ interactions, leading to B.E. = 55–70 MeV and Γ = 95–110 MeV. Ikeda and Sato [6] also obtained B.E. = 79 MeV and Γ = 74 MeV in a similar Faddeev calculation with a chiral SU(3)-based $\bar{K}N$-πY interaction. On the other hand, some authors claimed B.E. $\simeq$ 20 MeV [7,11] with $\bar{K}N$ interactions based on the chiral unitary approach [13,14], which are less attractive than the phenomenological $\bar{K}N$ interactions in the bound-state region. The discrepancy among theoretical results perhaps stems from the ambiguity of the $\bar{K}N$ interaction, together with the different procedures for three-body calculations involving decay processes. Further theoretical investigations are apparently needed.

Recently, several experimental observations of the K^-pp state have been reported. Data from the FINUDA Collaboration at DAΦNE [15] suggested evidence of a deeply bound K^-pp state in invariant-mass spectroscopy from stopped K^- reactions on ^{6}Li, ^{7}Li, and ^{12}C. Their measured energy and width are B.E. = 115 ± 9 MeV and $\Gamma = 67^{+16}_{-14}$ MeV, respectively. However, Magas *et al.* [16] claimed that the FINUDA data can be explained without postulating the existence of the K^-pp bound state. The OBELIX experiment at LEAR-CERN [17] also suggested observation of the K^-pp state in invariant-mass spectroscopy from stopped $\bar{p}$ reactions on ^{4}He. Very recently, Yamazaki *et al.* [18] found new experimental evidence of the K^-pp state in $p + p \to K^+ + \Lambda + p$ reactions in a reanalysis of old DISTO experimental data at SATURNE-Saclay. However, these experimental results also leave room for other interpretations and therefore more experimental data are required to confirm whether or not the K^-pp system has a deeply bound state.

Iwasaki *et al.* [19] have proposed a new experiment searching for the deeply bound K^-pp state at J-PARC using the missing-mass spectrum of the ^{3}He(in-flight K^-,n) reaction, together with invariant-mass spectra detecting all particles via decay processes from the K^-pp bound state (J-PARC E15 experiment). Moreover, a measurement of the K^-pp state in $p + p$ collisions has been planned by the FOPI Collaboration at GSI [20], as proposed by Yamazaki and Akaishi [21]. A search for light $\bar{K}$ nuclear systems involving the K^-pp state in stopped K^- reactions on ^{3}He/^{4}He targets has also been planned by the AMADEUS Collaboration at DAΦNE [22].

*tkoike@riken.jp

†harada@isc.osakac.ac.jp

Our purpose is to theoretically clarify the expected inclusive and semiexclusive spectra for the ^{3}He(in-flight K^-,n) reaction for the forthcoming J-PARC E15 experiment. In a previous work [23], we examined these spectra of the ^{3}He(in-flight K^-,n) reaction within a distorted-wave impulse approximation (DWIA) employing the Green's function method [24], which well describes unstable hadron systems [25]. It has been shown that the ^{3}He(in-flight K^-,n) reaction provides a promising spectrum that contains an s-wave dominance in the K^- bound region, where a strong nuclear distortion for K^- is reduced [23]. This is a major advantage of the use of an s-shell nuclear target such as ^{3}He. A similar calculation for the ^{3}He target is also presented by Yamagata *et al.* [11] using the chiral unitary approach. Investigations of heavier targets within a similar framework have been reported in several publications [26–29]. In the case of p-shell targets of ^{12}C and ^{16}O [26], signals of $\bar{K}$ nuclear states would not be extracted owing to their broad widths even if the bound states exist [27,28].

In this paper, we theoretically investigate the formation and decay of a deeply bound K^-pp state by the ^{3}He(in-flight K^-,n) reaction at incident K^- momentum $p_{K^-} = 1.0\,\mathrm{GeV}/c$ and forward direction $\theta_{\mathrm{lab}} = 0^\circ$ within a DWIA. To search for a signal of the deeply bound K^-pp state, we examine the inclusive and semiexclusive spectra including one-nucleon K^- absorption processes,

$$[K^-pp] \to \text{“}K^-p\text{”} + p \to \pi + Y + N, \tag{1}$$

and two-nucleon K^- absorption processes,

$$[K^-pp] \to K^- + \text{“}pp\text{”} \to Y + N, \tag{2}$$

near the $\pi\Sigma N$ decay threshold, where $Y = \{\Sigma, \Lambda\}$. Because many predictions of the B.E. and Γ for the K^-pp state exist at present, we demonstrate typical spectra by using the K^--“pp” optical potential, which reproduces the values of each B.E. and Γ phenomenologically. Here we employ the phenomenological K^--“pp” optical potentials having an energy dependence owing to the phase space factors of processes (1) and (2). If the B.E. is higher than about 100 MeV, a decay channel via process (1) with $Y = \Sigma$ is kinematically closed, so the decay width of the K^-pp bound state would be very small. Indeed, recent Faddeev calculations [5,6] and several experimental observations [15,18] have suggested that the B.E. is close to the energy at the $\pi\Sigma N$ decay threshold. To deal with this threshold effect, we must take into account the energy dependence of the K^--“pp” optical potential. This is a natural extension of previous work [23], where we mainly discussed spectra with an energy-independent optical potential. A preliminary result on this subject is partially reported in Ref. [30].

The outline of this paper is as follows. In Sec. II, we present our DWIA framework using the Green's function method for the ^{3}He(in-flight K^-,n) reaction, and we introduce several phenomenological energy-dependent K^--“pp” optical potentials, whose parameters are determined to reproduce the values of B.E. and Γ obtained from recent few-body calculations [4,5,7] or experimental candidates [15,17,18]. In Sec. III, we report the calculated inclusive and semiexclusive spectra for each optical potential. We find a distinct peak structure or cusplike structure at the $\pi\Sigma N$ threshold in the spectrum, depending on the potential parameters; the shape behavior of the spectrum is governed by a pole trajectory for the K^-pp state in the complex energy plane. In Sec. IV, we discuss the dependence of the spectral shape on the potential parameters and the branching ratio of K^- absorptions systematically, to clarify the appearance of the cusplike spectrum. A summary and conclusion are given in Sec. V.

II. FRAMEWORK

A. Distorted-wave impulse approximation

In the DWIA framework [31], the inclusive double-differential cross section of the ^{3}He(in-flight K^-,n) reaction in the forward direction $\theta_{\mathrm{lab}} = 0^\circ$ in the laboratory system is written [32] as

$$\frac{d^2\sigma}{dE_n d\Omega_n} = \beta(0^\circ)\left\langle \frac{d\sigma}{d\Omega_n}(0^\circ)\right\rangle_{\mathrm{lab}}^{K^-N\to N\bar{K}} S(E), \tag{3}$$

where $S(E)$ is a strength function of the K^-pp system as a function of the energy E, and $\langle d\sigma/d\Omega_n(0^\circ)\rangle_{\mathrm{lab}}^{K^-N\to N\bar{K}}$ is a Fermi-averaged cross section of the elementary $K^- + N \to N + \bar{K}$ forward scattering, which is equivalent to the backward $\bar{K} + N$ elastic scattering in the laboratory system [33]. The laboratory cross section for the non-spin-flip $K^- + n \to n + K^-$ ($K^- + p \to n + \bar{K}^0$) process amounts to 24.5 mb/sr (13.1 mb/sr) in free space [33,34] and is reduced to 13.9 mb/sr (7.5 mb/sr) with Fermi averaging [28,35]. Both the $K^- + n \to n + K^-$ elastic scattering and the $K^- + p \to n + \bar{K}^0$ charge exchange reaction can contribute to the formation of the K^-pp $I = 1/2$ state through coupling between K^-pp and $\bar{K}^0pn$ channels. Thus an incoherent sum of contributions from these $K^- + n \to n + K^-$ and $K^- + p \to n + \bar{K}^0$ processes, as used in Ref. [11], may be unsuitable for the K^-pp bound region. On the $\bar{K}^0/K^-$ charge basis, a coupled-channel calculation would be needed.

Here we consider the cross section of Eq. (3) on the isospin basis because total isospin $I = 1/2$ is expected to be an almost-good quantum number in the K^-pp bound state. The contribution from elementary processes is approximately estimated by the isoscalar $\Delta I = 0$ transition amplitude $f_{\Delta I=0} = -\sqrt{\frac{2}{3}}(f_{K^-n\to nK^-} + \frac{1}{2}f_{K^-p\to n\bar{K}^0})$ including a spectroscopic factor for the K^-pp $I = 1/2$ state formed on ^{3}He [28]. If we use the amplitude $f_{\Delta I=0}$ with Fermi averaging at $p_{K^-} = 1.0\,\mathrm{GeV}/c$ and $\theta_{\mathrm{lab}} = 0^\circ$, the Fermi-averaged cross section $\langle d\sigma/d\Omega_N(0^\circ)\rangle_{\mathrm{lab}}^{\Delta I=0} = |\langle f_{\Delta I=0}\rangle|^2$ is found to be 16.4 mb/sr, whereas this value is 1.2 mb/sr for the isovector $\Delta I = 1$ transition [28]. In our calculations, therefore, we adopt 16.4 mb/sr as the value of $\langle d\sigma/d\Omega_n(0^\circ)\rangle_{\mathrm{lab}}^{K^-N\to N\bar{K}}$ in Eq. (3).

The kinematic factor $\beta(0^\circ)$ [28,32] in Eq. (3) expresses the translation from the two-body K^--n laboratory system to the K^--^{3}He laboratory system at $\theta_{\mathrm{lab}} = 0^\circ$ [36], and it is defined as

$$\beta(0^\circ) = \left[1 - \frac{E_n^{(0)}}{E_{K^-}^{(0)}}\frac{p_{K^-} - p_n^{(0)}}{p_n^{(0)}}\right]\frac{p_n E_n}{p_n^{(0)} E_n^{(0)}}, \tag{4}$$

where p_{K^-} and p_n (E_{K^-} and E_n) are momenta of the incident K^- and the emitting n (energies of the residual K^- and the emitting n in the final state) in the many-body $K^- + {}^3\mathrm{He} \to n + [K^- pp]$ reaction, respectively, and the quantities with a (0) superscript are in the two-body $K^- + n \to n + K^-$ reaction. Note that the momentum transfer of this reaction becomes negative; $q(0^\circ) \equiv p_{K^-} - p_n < 0$. For negative momentum transfer, $\beta(0^\circ)$ enhances the spectrum of Eq. (3) by a factor of 1–2 , depending on p_n and E_{K^-} [28].

The strength function of the $K^- pp$ system, $S(E)$, in Eq. (3) can be given as a function of the energy E measured from the $K^- + p + p$ threshold:

$$E = M_{K^- pp} - (M_{K^-} + M_p + M_p), \tag{5}$$

where $M_{K^- pp}$, M_{K^-}, and M_p are the masses of the $K^- pp$ bound state, the K^-, and the proton, respectively. In this calculation, we assumed a "pp" pair to be a rigid core with a $^1S_0$ state. This assumption is suitable for qualitatively describing the structure of the $K^- pp$ state, as long as we consider the deeply bound region. A simple $(1s)^3$ harmonic oscillator model is used for the ^{3}He wave function, in which the relative $2N$-N wave function has the form $\phi_{2N\text{-}N}(r) \propto \exp(-r^2/2a^2)$, where $a = b_N\sqrt{\frac{3}{2}}$. The size parameter b_N is taken to be 1.30 fm, which reproduces the experimental root mean square charge radius of ^{3}He, $\sqrt{\langle r^2\rangle} = 1.94$ fm [37].

B. Green's function method

Here we consider Green's function for the $K^- pp$ system. It is obtained by solving the Klein-Gordon equation numerically:

$$\{[E - V_{\mathrm{Coul}}(\boldsymbol{r})]^2 + \nabla^2 - \mu^2 - 2\mu U^{\mathrm{opt}}(E;\boldsymbol{r})\}G(E;\boldsymbol{r},\boldsymbol{r}') = \delta^3(\boldsymbol{r} - \boldsymbol{r}'), \tag{6}$$

where μ is the reduced mass between the K^- and the "pp" core nucleus, and V_{Coul} is the Coulomb potential with the finite nuclear size effect. $U^{\mathrm{opt}}(E)$ is an energy-dependent K^--"pp" optical potential between the K^- and the "pp" core nucleus, which is assumed to be the Lorentz scalar type.

According to the Green's function method [24], we can write $S(E)$ as

$$S(E) = -\frac{1}{\pi}\,\mathrm{Im}\left[\sum_{\alpha,\alpha'}\int d\boldsymbol{r}d\boldsymbol{r}'\, f^\dagger_\alpha(\boldsymbol{r})G_{\alpha,\alpha'}(E;\boldsymbol{r},\boldsymbol{r}')f_{\alpha'}(\boldsymbol{r}')\right], \tag{7}$$

with

$$f_\alpha(\boldsymbol{r}) = \chi^{(-)*}\left(\boldsymbol{p}_n, \frac{M_{\mathrm{C}}}{M_{K^- pp}}\boldsymbol{r}\right) \times \chi^{(+)}\left(\boldsymbol{p}_{K^-}, \frac{M_{\mathrm{C}}}{M_{\mathrm{A}}}\boldsymbol{r}\right)\langle\alpha|\psi_n(\boldsymbol{r})|i\rangle, \tag{8}$$

where $G_{\alpha,\alpha'}(E)$ is the complete Green's function for the $K^- pp$ system, and $\langle\alpha|\psi_n(\boldsymbol{r})|i\rangle$ is the $2N$-N wave function for a struck neutron in the target, where α denotes the complete set of eigenstates for the system. $\chi^{(+)}$ and $\chi^{(-)}$ are distorted waves of the incoming K^-, with momentum $\boldsymbol{p}_{K^-}$, and the outgoing n, with momentum $\boldsymbol{p}_n$, respectively. The factors $M_{\mathrm{C}}/M_{K^- pp}$ and $M_{\mathrm{C}}/M_{\mathrm{A}}$ in Eq. (8) take into account the recoil effects, where M_{C} and M_{A} are the masses of the "pp" core nucleus and the ^{3}He target, respectively. The recoil effects have to moderate the whole shape of the spectrum. Indeed, if the recoil factors are omitted, the cross section of a peak in the bound region is reduced by about 50%; the yield in the quasifree (QF) region increases; and the QF peak is shifted upward to the higher-energy side, and its width is broader. Here we actually use the factor $M_{\mathrm{C}}/M_{K^- pp}$ not only in $\chi^{(-)}$ but also in $\chi^{(+)}$ for simplicity. If we use the alternative factor $M_{\mathrm{C}}/\bar{M}_{AK}$, where $\bar{M}_{AK}$ is the mean mass of M_{A} and $M_{K^- pp}$, instead of $M_{\mathrm{C}}/M_{K^- pp}$, we find that the cross section of the peak in the bound region is enhanced by less than 10%.

Using the Green's function technique, the strength function $S(E)$ for the inclusive spectrum can easily be decomposed into two parts [23,24]:

$$S(E) = S^{\mathrm{con}}(E) + S^{\mathrm{esc}}(E), \tag{9}$$

where $S^{\mathrm{con}}(E)$ denotes the K^- conversion processes including the decay modes of $[K^- pp] \to \pi + Y + N$ and $[K^- pp] \to Y + N$, which come from the one- and two-nucleon K^- absorptions in Eqs. (1) and (2), respectively; and S^{esc}(E) denotes the K^- escape processes, where the K^- leaves from the core nucleus as $[K^- pp] \to K^-$+ "pp" above the $K^- + p + p$ threshold ($E > 0$). Using abbreviated notation for $G(E)$, $U^{\mathrm{opt}}(E)$, and f, instead of that in Eq. (7), we have

$$S^{\mathrm{con}}(E) = -\frac{1}{\pi}\langle f^\dagger G^\dagger(E)\{\mathrm{Im}\ U^{\mathrm{opt}}(E)\}G(E)f\rangle, \tag{10}$$

$$S^{\mathrm{esc}}(E) = -\frac{1}{\pi}\langle f^\dagger[1 + G^\dagger(E)U^{\mathrm{opt}\dagger}(E)] \times \{\mathrm{Im}\ G_0(E)\}[1 + U^{\mathrm{opt}}(E)G(E)]f\rangle, \tag{11}$$

where $G_0(E)$ is the free Green's function.

With the help of the eikonal approximation, we express the distorted waves in Eq. (8) as

$$\chi^{(-)*}(\boldsymbol{p}_n,\boldsymbol{r}) = \exp\left[-i\boldsymbol{p}_n\cdot\boldsymbol{r} - \frac{i}{v_n}\int_z^{+\infty} U_n(\boldsymbol{b},z')dz'\right], \tag{12}$$

$$\chi^{(+)}(\boldsymbol{p}_{K^-},\boldsymbol{r}) = \exp\left[+i\boldsymbol{p}_{K^-}\cdot\boldsymbol{r} - \frac{i}{v_{K^-}}\int_{-\infty}^{z} U_{K^-}(\boldsymbol{b},z')dz'\right], \tag{13}$$

with the impact parameter coordinate $\boldsymbol{b}$ and the optical potential for $\lambda = K^-$ or n,

$$U_\lambda(r) = -i\frac{v_\lambda}{2}\bar{\sigma}^{\mathrm{tot}}_{\lambda N}(1 - i\alpha_{\lambda N})\rho(r), \tag{14}$$

where $\rho(r)$ is the nuclear density distribution, and $\bar{\sigma}^{\mathrm{tot}}_{\lambda N}$ and $\alpha_{\lambda N}$ denote the isospin-averaged total cross section and the ratio of the real to the imaginary parts of the forward amplitude for $\lambda + N$ scattering, respectively. At $p_{K^-} = 1.0\,\mathrm{GeV}/c$, the total cross sections of $\sigma^{\mathrm{tot}}_{K^- p}$ and $\sigma^{\mathrm{tot}}_{K^- n}$ amount to ~50 and ~40 mb, respectively, and $\sigma^{\mathrm{tot}}_{np}$ varies within 30–40 mb in the corresponding momenta $p_n = 1.1$–$1.4\,\mathrm{MeV}/c$ [38]. We confirm that the absolute values of the formation cross section in Eq. (3) are enhanced or reduced by up to about 20% when the values of $\bar{\sigma}^{\mathrm{tot}}_{\lambda N}$ are changed within 30–50 mb, but the whole

shape of the spectrum is hardly modified. Thus we use $\bar{\sigma}^{\rm tot}_{K^-N} = \bar{\sigma}^{\rm tot}_{nN} = 40$ mb [33,39] for simplicity. Because the formation cross section is rather insensitive to the values of $\alpha_{\lambda N}$ [40], we use $\alpha_{K^-N} = \alpha_{nN} = 0$ [33,39]. This fact implies that distortion effects are not very important in our calculation, because of the small nuclear size of the ^{3}He target. It has been shown that the distortion factor for the (in-flight K^-,n) reaction on ^{3}He is estimated as $D_{\rm dis} = 0.47$ for the $1s_p \to 1s_{K^-}$ transition [23]; this value is about five times as large as the $D_{\rm dis} = 0.095$ for the $1p_p \to 1s_{K^-}$ transition on a ^{12}C target [39]. This is also an advantage of the use of s-shell nuclear targets such as ^{3}He.

C. Optical potentials for the K^--"pp" system

In a previous paper [23], we evaluated spectra with an energy-independent K^--"pp" optical potential, which reproduced the results for the binding energy (B.E.) and width (Γ) obtained by Yamazaki and Akaishi [4] or by Shevchenko *et al.* [5]. On the other hand, Mareš, Friedman, and Gal [41] introduced the phase space suppression factors $f_1^Y(E)$ and $f_2^Y(E)$, which denote, for the one- and two-nucleon K^- absorption processes, respectively,

$$f_1^Y(E) = \frac{M_1^3(0)}{M_1^3(E)} \times \sqrt{\frac{\left[M_1^2(E) - (M_Y + M_\pi)^2\right]\left[M_1^2(E) - (M_Y - M_\pi)^2\right]}{\left[M_1^2(0) - (M_Y + M_\pi)^2\right]\left[M_1^2(0) - (M_Y - M_\pi)^2\right]}} \times \Theta[M_1(E) - M_Y - M_\pi], \quad (15)$$

$$f_2^Y(E) = \frac{M_2^3(0)}{M_2^3(E)} \times \sqrt{\frac{\left[M_2^2(E) - (M_Y + M_N)^2\right]\left[M_2^2(E) - (M_Y - M_N)^2\right]}{\left[M_2^2(0) - (M_Y + M_N)^2\right]\left[M_2^2(0) - (M_Y - M_N)^2\right]}} \times \Theta[M_2(E) - M_Y - M_N], \quad (16)$$

with $M_1(E) = M_{\bar{K}} + M_N + E$ and $M_2(E) = M_{\bar{K}} + 2M_N + E$, where $M_{\bar{K}}$, M_N, M_Y, and M_π denote the masses of the $\bar{K}$, nucleon, hyperon ($Y = \Sigma$ or Λ), and π, respectively; $\Theta(x) = 1$ for $x \geqslant 0$ and 0 for $x < 0$. Figure 1 displays these phase space suppression factors as a function of E. $f_1^\Sigma(E)$ vanishes below the $\pi\Sigma N$ threshold of $E_{\rm th}(\pi\Sigma N) = -101$ MeV, and $f_1^\Lambda(E)$ vanishes below the $\pi\Lambda N$ threshold of $E_{\rm th}(\pi\Lambda N) = -181$ MeV. $f_2^Y(E)$ vanishes below the YN threshold, for example, $E_{\rm th}(\Sigma N) = -239$ MeV or $E_{\rm th}(\Lambda N) = -319$ MeV. As attempted in Refs. [26] and [27], we take into account the energy dependence of the imaginary part multiplied by $f_1^Y(E)$ or $f_2^Y(E)$ in the optical potential. Thus we employ the energy-dependent K^--"pp" optical potential, which is parametrized in Gaussian form, with a range parameter b, as

$$U^{\rm opt}(E;\boldsymbol{r}) = [V_0 + iW_0 f(E)]\exp[-(\boldsymbol{r}/b)^2], \quad (17)$$

with

$$f(E) = B_1^{(\pi\Sigma N)} f_1^\Sigma(E) + B_1^{(\pi\Lambda N)} f_1^\Lambda(E) + B_2^{(YN)} f_2^Y(E), \quad (18)$$

where V_0 and W_0 are adjusted parameters whose values are determined to reproduce the results for the binding energy and width of the K^-pp state in theoretical predictions or experimental data, as we mention later. $B_1^{(\pi\Sigma N)}$ and $B_1^{(\pi\Lambda N)}$ are branching rates to $[K^-pp] \to \pi + \Sigma + N$ and $[K^-pp] \to \pi + \Lambda + N$ decay channels from one-nucleon K^- absorption, respectively, and $B_2^{(YN)}$ is the branching rate to the $[K^-pp] \to Y + N$ decay channel from two-nucleon K^- absorption. Here we assumed [27,41,42]

$$B_1^{(\pi\Sigma N)} = 0.7, \quad B_1^{(\pi\Lambda N)} = 0.1, \quad B_2^{(YN)} = 0.2, \quad (19)$$

where we take that the $[K^-pp] \to Y + N$ process acts effectively in the $\Sigma + N$ and $\Lambda + N$ decay channels because these channels similarly affect the spectrum within the present framework (see also Fig. 1). Then we can rewrite the imaginary part of $U^{\rm opt}(E)$ in Eq. (17) as

$$\mathrm{Im}\, U^{\rm opt}(E;\boldsymbol{r}) = W_1^\Sigma(E;\boldsymbol{r}) + W_1^\Lambda(E;\boldsymbol{r}) + W_2^Y(E;\boldsymbol{r}), \quad (20)$$

where $W_1^Y(E;\boldsymbol{r})$ and $W_2^Y(E;\boldsymbol{r})$ correspond to the absorptive potentials for one- and two-nucleon K^- absorptions, respectively:

$$W_1^Y(E;\boldsymbol{r}) = B_1^{(\pi YN)} W_0 f_1^Y(E)\exp[-(\boldsymbol{r}/b)^2], \quad (21)$$

$$W_2^Y(E;\boldsymbol{r}) = B_2^{(YN)} W_0 f_2^Y(E)\exp[-(\boldsymbol{r}/b)^2]. \quad (22)$$

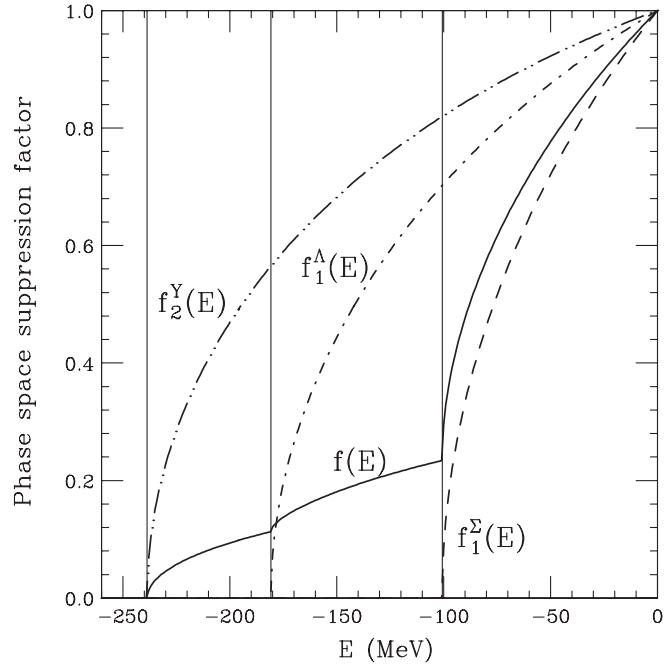

FIG. 1. Phase space suppression factors introduced by Mareš *et al.* [41], as a function of E. Dashed and dash-dotted curves denote the phase space factors $f_1^\Sigma(E)$ for the $[K^-pp] \to \pi + \Sigma + N$ process and $f_1^\Lambda(E)$ for the $[K^-pp] \to \pi + \Lambda + N$ process, respectively, from one-nucleon K^- absorption. The dash-dot-dotted curve denotes $f_2^Y(E)$ for the $[K^-pp] \to Y + N$ process from two-nucleon K^- absorption. The solid curve denotes the total phase space factor $f(E) = B_1^{(\pi\Sigma N)} f_1^\Sigma(E) + B_1^{(\pi\Lambda N)} f_1^\Lambda(E) + B_2^{(YN)} f_2^Y(E)$, where $[B_1^{(\pi\Sigma N)}, B_1^{(\pi\Lambda N)}, B_2^{(YN)}] = (0.7, 0.1, 0.2)$ is assumed. The vertical lines at $E \simeq -100$, -180, and -240 MeV indicate the $\pi + \Sigma + N$, $\pi + \Lambda + N$, and $Y + N$ decay threshold energies, respectively.

In the Green's function method, $S^{\rm con}(E)$ in Eq. (10) can be further decomposed [23] as

$$S^{\rm con}(E) = S^{\rm con}_{\pi\Sigma N}(E) + S^{\rm con}_{\pi\Lambda N}(E) + S^{\rm con}_{YN}(E), \qquad (23)$$

with

$$S^{\rm con}_{\pi YN}(E) = -\frac{1}{\pi}\left\langle f^\dagger G^\dagger(E) W_1^Y(E) G(E) f\right\rangle, \qquad (24)$$

$$S^{\rm con}_{YN}(E) = -\frac{1}{\pi}\left\langle f^\dagger G^\dagger(E) W_2^Y(E) G(E) f\right\rangle, \qquad (25)$$

where $S^{\rm con}_{\pi YN}(E)$ and $S^{\rm con}_{YN}(E)$ express components of the strength functions for the $\pi + Y + N$ decay process from one-nucleon K^- absorption and for the $Y + N$ decay process from two-nucleon K^- absorption, respectively, in the K^- conversion spectra. Therefore, the semiexclusive spectra in the ^{3}He(in-flight K^-,n) reaction,

$$K^- + {}^3{\rm He} \to n + [K^- pp] \to n + Y + X, \qquad (26)$$

can be evaluated in our calculations, where $Y = \{\Sigma, \Lambda\}$ and $X = \{\pi + N, N\}$.

The binding energies B.E. and widths Γ of the $K^- pp$ bound state with $I = 1/2$, $J^\pi = 0^-$, have been predicted in many calculations [5–12] and also reported in several experiments [15,17,18]. In Fig. 2, we summarize the values of

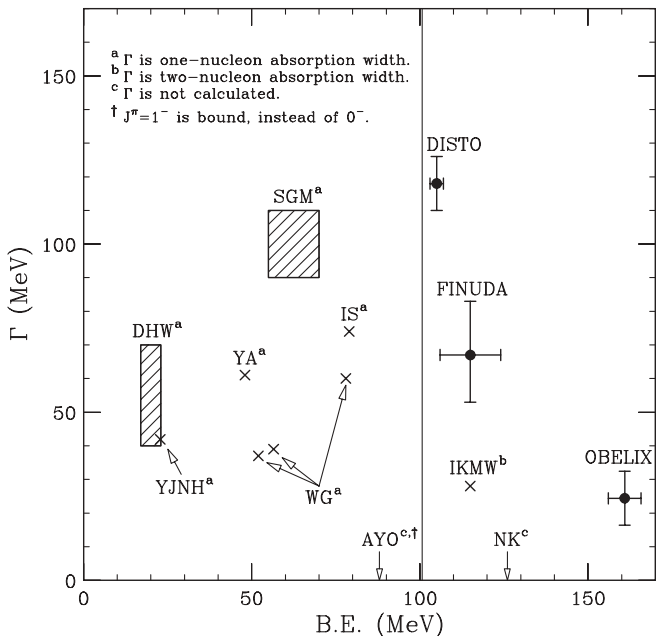

FIG. 2. Summary of binding energies and widths of the $K^- pp$ bound state. Theoretical calculations for the $I = 1/2$, $J^\pi = 0^-$, state were predicted by YA (Yamazaki and Akaishi) [4], SGM (Shevchenko, Gal, and Mareš) [5], IS (Ikeda and Sato) [6], DHW (Doté, Hyodo, and Weise) [7], IKMW (Ivanov *et al.*) [8], NK (Nishikawa and Kondo) [9], YJNH (Yamagata *et al.*) [11], and WG (Wycech and Green) [12]; calculations for the $I = 1/2$, $J^\pi = 1^-$ state by AYO (Arai, Oka, and Yasui) [10]. Data were taken from the FINUDA [15], OBELIX [17], and DISTO [18] experiments. The vertical line at B.E. $\simeq$ 100 MeV indicates the $\pi\Sigma N$ decay threshold.

B.E. and Γ taken from theoretical predictions and experimental candidates. By taking these results for B.E. and Γ as a guide, we attempt to construct the K^--"pp" optical potentials $U^{\rm opt}(E)$. We solve the Klein-Gordon equation self-consistently in the complex energy plane:

$$\{[\omega(E) - V_{\rm Coul}(\boldsymbol{r})]^2 + \nabla^2 - \mu^2 - 2\mu U^{\rm opt}(E;\boldsymbol{r})\}\Phi(E;\boldsymbol{r}) = 0, \qquad (27)$$

where $\Phi(E;\boldsymbol{r})$ is a relative wave function between the K^- and the "pp" core nucleus, and $\omega(E)$ is a complex eigenvalue, as a function of E, which is a real number. If we find that E satisfies

$$\mathrm{Re}\ \omega(E) = E, \qquad (28)$$

we can obtain Re $\omega(E) = -$B.E. and Im $\omega(E) = -\Gamma/2$ as the Klein-Gordon complex energy. Thus we determine the strength parameters (V_0, W_0) in Eq. (17) by fitting to the prediction of or candidate for B.E. and Γ. Here we introduce four K^--"pp" optical potentials $U^{\rm opt}(E)$ as follows:

(i) Potential A was determined by fitting to B.E. $\simeq$ 20 MeV and a maximum $\Gamma \simeq$ 70 MeV in a variational three-body calculation based on the chiral unitary approach of Doté, Hyodo, and Weise [7].

(ii) Potential B, which is equivalent to the energy-independent optical potential obtained in the variational three-body calculation by Yamazaki and Akaishi [4], was determined by fitting to B.E. = 48 MeV and Γ = 61 MeV.

(iii) Potential C was determined by fitting to B.E. $\simeq$ 70 MeV and $\Gamma \simeq$ 110 MeV in the $\bar{K}NN$-$\pi\Sigma N$ coupled-channel Faddeev calculation of Shevchenko *et al.* [5]. These values correspond to the maximum B.E. and Γ, respectively, within the uncertainty of their results.

(iv) Potential D is a series of the potentials we determined by fitting to the experimental observations for B.E. and Γ: D_1, D_2, and D_3 indicate the potentials for the DISTO [18], FINUDA [15], and OBELIX [17] experiments, respectively.

For the range parameter for $U^{\rm opt}(E)$ in Eq. (17), here we used $b = 1.09$ fm, a value derived from the results of three-body calculations by Yamazaki and Akaishi [4]. A slight dependence of the spectrum on the range parameter b is seen in the QF region; for example, when b is changed within +0.12 fm (−0.12 fm) in potential C, the cross section of the QF peak is reduced (enhanced) by less than 10% and its peak position is shifted within −5 MeV (+5 MeV), whereas the bound-state spectrum is almost unchanged. Note that the values of Γ that we considered in (i)–(iii) were obtained by microscopic three-body calculations with only $\pi + Y + N$ decay processes in one-nucleon K^- absorption [4,5,7]. Because the K^--"pp" optical potential has to describe not only one-nucleon, but also two-nucleon, K^- absorption processes, we employ the parameters (V_0, W_0) for potentials A, B, and C by fitting to the values of B.E. and Γ without $B_2^{(YN)}$ in Eq. (18), that is, $[B_1^{(\pi\Sigma N)}, B_1^{(\pi\Lambda N)}, B_2^{(YN)}] = (0.7, 0.1, 0.0)$. For potential D, we took the parameters with $B_2^{(YN)}$. In Table I, we list the parameter sets of (V_0, W_0) for $U^{\rm opt}(E)$, together

TABLE I. Parameters of the real and imaginary strengths, V_0 and W_0, of the K^--"pp" optical potentials $U^{\rm opt}(E;\boldsymbol{r})$ for the $I = 1/2$, $J^\pi = 0^-$, bound state in Eq. (17). The range parameter is $b = 1.09$ fm. Branching rates of the one-nucleon K^- absorption process are taken to be $B_1^{(\pi\Sigma N)} = 0.7$ and $B_1^{(\pi\Lambda N)} = 0.1$, respectively, and the branching rate of the two-nucleon K^- absorption process is $B_2^{(YN)} = 0.2$. Values in parentheses are for the imaginary parts of the energy-independent potentials $U_0^{\rm opt}(\boldsymbol{r})$. All values are in MeV.

Potential	V_0	W_0	Without $B_2^{(YN)}$		With $B_2^{(YN)}$		Ref.
			B.E.[a]	Γ[b]	B.E.[a]	Γ[c]	
A	−237	−128(−120)	21	70	15	92	DHW [7]
B	−292	−107(−86)	48	61	45	82	YA [4]
C	−344	−203(−147)	70	110	59	164	SGM [5]
D_1	−399	−372(−86)	114	34	105	118	DISTO [18]
D_2	−404	−213(−47)	118	19	115	67	FINUDA [15]
D_3	−458	−82(−13)	162	5	161	24	OBELIX [17]

[a]Binding energy of the K^-pp bound state measured from the $K^- + p + p$ threshold.
[b]Width of one-nucleon K^- absorption processes.
[c]Total width of one- and two-nucleon K^- absorption processes.

with their calculated binding energies B.E. and widths Γ for the K^-pp bound state. We find that when $B_2^{(YN)}$ is switched on, the values of B.E. decrease and those of Γ increase.

In Fig. 3, we display the real and imaginary parts of the K^--"pp" optical potentials $U^{\rm opt}(E)$ as a function of the distance between the K^- and the center of the "pp" core nucleus. If we neglect the energy dependence of $U^{\rm opt}(E)$ in Eq. (17) by replacing $f(E)$ with 1, we find the energy-independent optical potentials $U_0^{\rm opt}$, as used in our previous calculations [23]. It should be noted that the values of W_0 in $U_0^{\rm opt}$ differ from those in $U^{\rm opt}(E)$, as reported in Table I, whereas we have Im $U_0^{\rm opt}$ = Im $U^{\rm opt}(E)$ at $E = -$B.E.

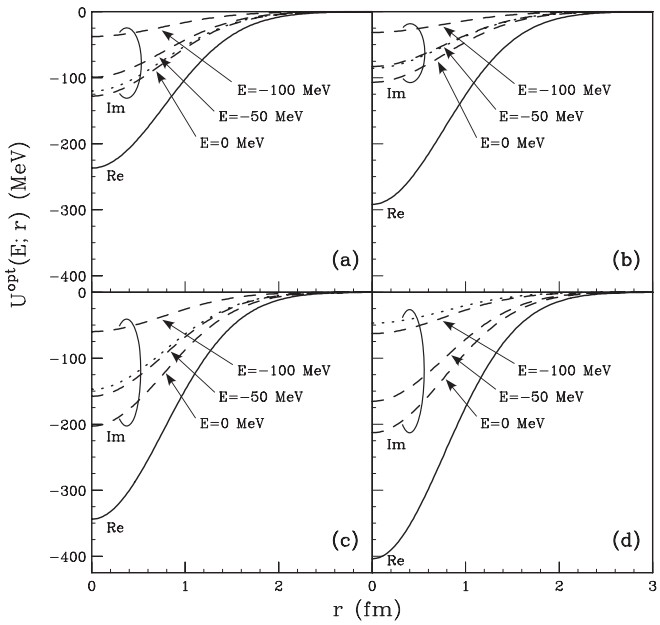

FIG. 3. Real and imaginary parts of the K^--"pp" optical potentials $U^{\rm opt}(E;\boldsymbol{r})$ for potentials (a) A, (b) B, (c) C, and (d) D_2, as a function of the distance between K^- and the center of the "pp" core nucleus. Solid curves denote the real parts, and dashed curves the imaginary parts, at $E = 0, -50$, and -100 MeV. Dotted curves denote the imaginary parts for the energy-independent K^--"pp" optical potentials $U_0^{\rm opt}(\boldsymbol{r})$.

III. NUMERICAL RESULTS

A. Inclusive spectrum for the ^{3}He(in-flight K^-,n) reaction

Let us consider the ^{3}He(in-flight K^-,n) reaction at $p_{K^-} = 1.0\,{\rm GeV}/c$ and $\theta_{\rm lab} = 0^\circ$ for the J-PARC E15 experiment [19]. To find possible evidence of the K^-pp bound state, we evaluate the inclusive and semiexclusive spectra of the ^{3}He(in-flight K^-,n) reaction numerically using Eqs. (3), (9)–(11), and (23)–(25).

In Fig. 4, we display the calculated results for the inclusive spectra with the optical potentials $U^{\rm opt}(E)$ listed in Table I. In Fig. 4(c), we show the calculated inclusive spectrum for potential C, where the binding energy and width of the K^-pp bound state were obtained as B.E. = 59 MeV and Γ = 164 MeV, respectively. The inclusive spectrum with $U^{\rm opt}(E)$ is qualitatively different from that with the energy-independent $U_0^{\rm opt}$. The former has a cusp that appears at the $\pi\Sigma N$ threshold in the $L = 0$ component of the spectrum, whereas the latter has no peak because of the large width of the K^-pp state [23]. This cusplike structure originates from the energy dependence of the imaginary part of $U^{\rm opt}(E)$, and its mechanism can be understood by the behavior of a pole trajectory of the K^-pp state in the complex energy plane, as discussed in Sec. III C.

In Fig. 4(b), we show the inclusive spectrum for potential B, which gives B.E. = 45 MeV and Γ = 82 MeV. A clear peak of the K^-pp state appears in both the spectrum with $U^{\rm opt}(E)$ and that with $U_0^{\rm opt}$, but the peak position for $U^{\rm opt}(E)$ is shifted slightly, from $E = -45$ MeV to $E = -50$ MeV, because of its energy dependence. Because this state is away from the branching point of the $\pi\Sigma N$ threshold, the peak in the spectrum is scarcely influenced by the threshold, so that its shape approximately indicates a standard Breit-Wigner (BW) form [28]. As the $\pi\Sigma N$ phase space is taken into account, the spectrum for $U^{\rm opt}(E)$ is suppressed below the $\pi\Sigma N$ decay threshold of $E_{\rm th}(\pi\Sigma N) \simeq -100$ MeV, in contrast to that for $U_0^{\rm opt}$ [23].

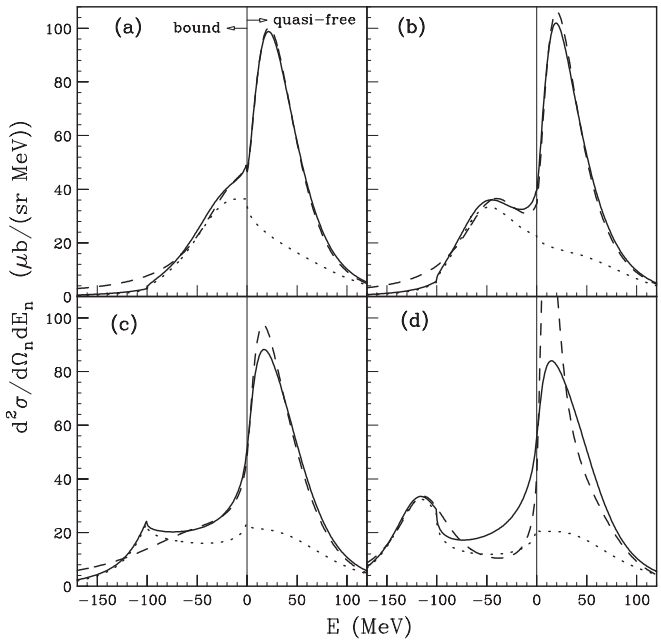

FIG. 4. Calculated inclusive spectra for the ^{3}He(in-flight K^-,n) reaction at $p_{K^-} = 1.0\,\mathrm{GeV}/c$ and $\theta_{\mathrm{lab}} = 0^\circ$ as a function of the energy E of the K^-pp system measured from the $K^- + p + p$ threshold for potentials (a) A, (b) B, (c) C, and (d) D_2. Solid and dashed curves denote the inclusive spectra for the energy-dependent $U^{\mathrm{opt}}(E)$ and energy-independent U_0^{opt} potentials, respectively. The dotted curve denotes the $L = 0$ component in the inclusive spectrum for $U^{\mathrm{opt}}(E)$. The vertical line at $E = 0\,\mathrm{MeV}$ indicates the $K^- + p + p$ threshold, and the left- and right-hand sides of this line are the K^- bound and quasifree scattering regions, respectively.

Figure 4(a) shows that the peak of the K^-pp bound state is not clear in the inclusive spectrum with potential A, because of the relatively low binding energy of 15 MeV and the large width of 92 MeV. The energy dependence of the spectrum for $U^{\mathrm{opt}}(E)$ seems to be similar to that with potential B. Yamagata *et al.* [11] performed a similar calculation using the energy-dependent K^--"pp" optical potential based on the chiral unitary model. The shape of their inclusive spectrum is different from that of ours because of the different contribution of the partial-wave components and their different widths; they found the K^-pp $L = 0$ bound state with B.E. $\simeq 20\,\mathrm{MeV}$ and $\Gamma \simeq 40\,\mathrm{MeV}$, and other $L = 1$, 2 bound states with B.E. $\simeq$ 10 MeV [11]. However, it is not understood that the K^-pp system has nuclear bound states with $L \geqslant 1$, considering its small nuclear size such as for ^{3}He.[1]

We consider potential D_2 to be a typical example of the potential D series. In Fig. 4(d), we show the inclusive spectrum with potential D_2 by fits to the experimental values, B.E. = 115 MeV and $\Gamma = 67\,\mathrm{MeV}$, which were obtained from the invariant-mass spectrum in the FINUDA experiment [15]. If the interpretation of the FINIDA candidate as a K^-pp bound state is true, a clear peak should appear below the $\pi\Sigma N$ threshold in the missing-mass spectrum. It would be easy to observe such a peak structure experimentally. The spectra with $U^{\mathrm{opt}}(E)$ and U_0^{opt} are quite similar in shape below the $\pi\Sigma N$ threshold, whereas they differ considerably above the $\pi\Sigma N$ threshold. For potentials D_1 and D_3, which were determined by fits to the DISTO [18] and OBELIX [17] data, respectively, we also see that a clear peak in the spectra appears below the $\pi\Sigma N$ threshold (see also Fig. 10). We find that the shape of the peak in the spectrum with D_1 is similar to that in the spectrum with D_2, as shown in Fig. 4(d), whereas the spectrum with D_3 has a very prominent peak because of the small width of $\Gamma = 24\,\mathrm{MeV}$.

Therefore, we recognize that the inclusive spectrum of the ^{3}He(in-flight K^-,n) reaction at $p_{K^-} = 1.0\,\mathrm{GeV}/c$ and $\theta_{\mathrm{lab}} = 0^\circ$ is expected to have a signal for clear evidence of the K^-pp bound state. The calculated spectrum predominantly has a bound state with $I = 1/2$, $J^\pi = 0^-$, and an orbital angular momentum $L = 0$ in the K^-pp bound region below the $K^- + p + p$ threshold, whereas continuum states with $L \geqslant 1$ occur in the QF region. We stress that the (in-flight K^-, n) reaction on an s-shell nuclear target such as ^{3}He provides an advantage in producing a deeply bound K^- nuclear state with $L = 0$. These results also indicate the importance of energy dependence of the K^--"pp" optical potentials, particularly in the case of potentials C, D_1, and D_2. We realize the limit for applying the energy-independent optical potential to calculations of the spectrum; this potential can be justified only for potential A, involving shallow potentials [7,11], and it works approximately for potential B around the K^-pp peak. The strength of $|V_0|$ in U_0^{opt} must be shallower than 300 MeV, which corresponds to B.E. $< 50\,\mathrm{MeV}$.

B. Contribution of one- and two-nucleon K^- absorption processes in K^- conversion spectra

It should be noted that the calculated K^- conversion spectra can be directly compared with the experimental data from the J-PARC E15 experiment, which is planned to measure (in-flight K^-,n) spectra and decaying particles from the K^-pp system simultaneously [19]; no K^- escape spectrum will be measured in this experiment. To search for a better signal of the K^-pp bound state, we focus on the K^- conversion spectra that express semiexclusive $K^- + {}^3\mathrm{He} \to n + Y + X$ processes in the deeply bound region, where $Y = \{\Sigma, \Lambda\}$ and $X = \{\pi + N, N\}$. By Eqs. (24) and (25), we can calculate the strength functions for K^- conversion processes, which are effectively described by the imaginary potential Im $U^{\mathrm{opt}}(E)$ in Eq. (20), within the optical models. For K^- escape processes, we can calculate the strength function in Eq. (11), which is probably underestimated because it is described as K^- + "pp" continuum states above the $K^- + pp$ threshold, where "pp" should actually break up into $p + p$.

In Fig. 5, we illustrate partial contributions in the ^{3}He(in-flight K^-,n) spectrum at $p_{K^-} = 1.0\,\mathrm{GeV}/c$ and $\theta_{\mathrm{lab}} = 0^\circ$, for example, the $[K^-pp] \to \pi + \Sigma + N$ decay process and $[K^-pp] \to \pi + \Lambda + N$ decay process from one-nucleon K^- absorption and the $[K^-pp] \to Y + N$ decay process from two-nucleon K^- absorption. Figure 5(c) shows that the

[1] In the Note Added in Proof in Ref. [11], it is commented that bound states with $L \geqslant 1$ should not be interpreted as the three-body K^-pp state but could be $\Lambda(1405)$ formed by the two-body K^-p state.

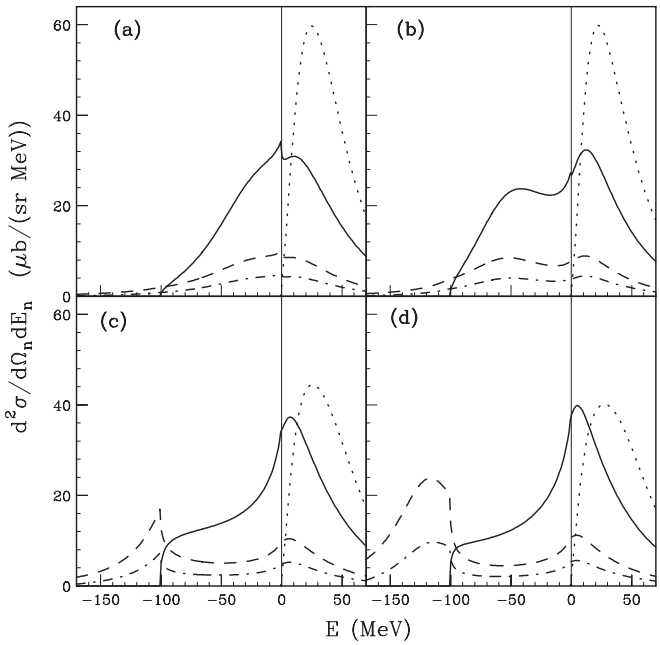

FIG. 5. Calculated semiexclusive spectra for the ^{3}He(in-flight K^-,n) reaction at $p_{K^-} = 1.0\,\mathrm{GeV}/c$ and $\theta_{\mathrm{lab}} = 0^\circ$, for potentials (a) A, (b) B, (c) C, and (d) D_2. Solid and dot-dashed curves denote the $[K^- pp] \to \pi + \Sigma + N$ and $\pi + \Lambda + N$ decay processes from one-nucleon K^- absorption, respectively. Dashed curves denote the $[K^- pp] \to Y + N$ decay process from two-nucleon K^- absorption. Dotted curves denote the spectra of the K^- escape process. See also the caption to Fig. 4.

cusplike peak at the $\pi\Sigma N$ threshold originates from the $\pi + \Lambda + N$ and $Y + N$ decay channels in the spectrum for potential C, rather than the $\pi + \Sigma + N$ decay channel, which is suppressed below the $\pi\Sigma N$ threshold because its decay channel is closed there. This cusplike peak is clear evidence of formation of the $K^- pp$ bound state. Because the observed peak position and width do not directly correspond to the actual binding energy and width, respectively, we need a comparison between the theoretical and the experimental spectra to extract the binding energy and width of the $K^- pp$ bound state from the cusplike peak.

In Fig. 5(d), it is also interesting to see the clear peak in the $\pi + \Lambda + N$ and $Y + N$ decay spectra with potential D_2, which is more attractive than potential C. Its shape is asymmetric because it must be sharply cut by the phase space suppression factor above the $\pi\Sigma N$ threshold. Moreover, we confirm that the $\pi + \Sigma + N$ decay spectrum gives no peak for the $K^- pp$ bound state, nor does the spectrum with potential C.

Figure 5(b) shows partial contributions in the calculated spectrum with potential B. We find that the shapes of the spectra with $\pi + \Sigma + N$, $\pi + \Lambda + N$, and $Y + N$ decay processes are essentially the same, but the peak positions of these spectra differ slightly because of the energy dependence of the potential. A clear signal would be observed in the spectrum with $[K^- pp] \to Y + N$ from two-nucleon K^- absorption, as well as the inclusive spectrum shown in Fig. 4(b).

On the other hand, we confirm that there is no peak in any partial contributions with potential A even though the $K^- pp$ bound state exists, as shown in Fig. 5(a). This state exists close to the $K^- + p + p$ threshold owing to the low binding energy, B.E. = 15 MeV, and the large width, $\Gamma = 92$ MeV. For a more quantitative estimation, we must examine the whole shape of the spectrum, including the effects of the $K^- + p + p$ threshold [24,28].

We recognize that a detailed comparison between the theoretical and the experimental spectra is required to extract the binding energy and width of the $K^- pp$ bound state from the spectra. The shape behavior of the $[K^- pp] \to \pi + \Lambda + N$ decay spectrum is quite similar to that of the $[K^- pp] \to Y + N$ spectrum with all of our potentials. This similarity is understood from the fact that the energy dependence of the phase space factor $f_1^\Lambda(E)$ for $\pi + \Lambda + N$ decay processes resembles that of $f_2^Y(E)$ for $Y + N$ decay processes near the $\pi\Sigma N$ threshold.

C. Pole trajectory for the deeply bound $K^- pp$ state

1. A moving pole in the complex energy plane

It is important to understand the mechanism of the peak structure near the $\pi\Sigma N$ threshold in the spectrum, so as to identify the nature of the $K^- pp$ bound state from the experimental data. Quantum mechanically, a peak structure in the energy spectrum is associated with a pole in the scattering amplitude or the complete Green's function. The pole position corresponds to a complex eigenvalue of a Hamiltonian on the complex energy plane. The shape of the spectrum must be modified by the threshold effects if the pole is located near the branch point of the threshold. To understand the shape behavior of the $[K^- pp] \to Y + N$ decay spectrum, we investigate the pole position of the $K^- pp$ state in the complex energy plane. We can obtain the pole position as a complex eigenvalue of $\omega(E)$ in Eq. (27), as a function of E, because of the energy dependence of $U^{\mathrm{opt}}(E)$.

The shape of the inclusive spectrum in the K^- bound region may perhaps be written in the following form:

$$S^{(\mathrm{pole})}(E) = -\frac{1}{\pi}\frac{\mathrm{Im}\,\omega(E)}{D^2(E)}, \tag{29}$$

where

$$D(E) \equiv \sqrt{[E - \mathrm{Re}\,\omega(E)]^2 + [\mathrm{Im}\,\omega(E)]^2} \tag{30}$$

denotes the distance between point $(E, 0)$ of the physical state on the real axis and the pole at point [Re $\omega(E)$, Im $\omega(E)$] in the complex energy plane, as illustrated in Fig. 6. If the energy dependence of $\omega(E)$ is negligible, the shape of $S^{(\mathrm{pole})}(E)$ is equivalent to the BW resonance form. Because Im $\omega(E)$ is approximately proportional to the phase space suppression factor $f(E)$, the shape of the inclusive spectrum is roughly denoted $f(E)/D^2(E)$. Functions $f_1^Y(E)/D^2(E)$ and $f_2^Y(E)/D^2(E)$ can simulate the shapes of the one- and two-nucleon K^- absorption spectra, respectively. It is apparent that $S^{\mathrm{con}}_{\pi\Sigma N}(E)$ is suppressed below the $\pi\Sigma N$ threshold owing to the behavior of the function $f_1^Y(E)$. On the contrary, $S^{\mathrm{con}}_{\pi\Lambda N}(E)$ and $S^{\mathrm{con}}_{YN}(E)$ are approximately equivalent to $1/D^2(E)$ because $f_1^\Lambda(E)$ and $f_2^Y(E)$ can be regarded as constants around the

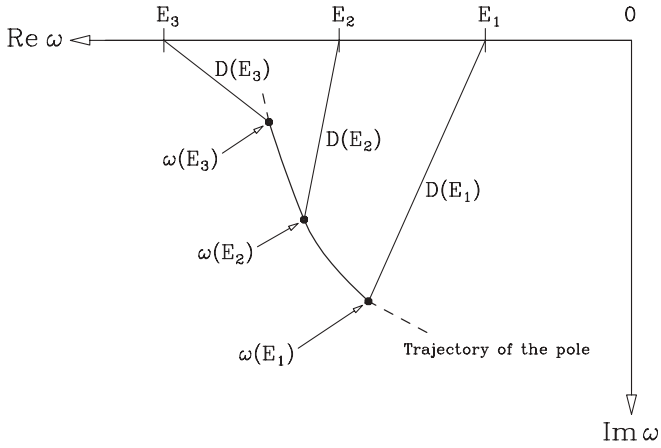

FIG. 6. Distance $D(E)$ between point $(E, 0)$ on the real axis and the pole at [Re $\omega(E)$, Im $\omega(E)$] for the $K^- pp$ state in the complex energy plane. The pole moves on the trajectory as a function of the real energy E. Some examples are illustrated at $E = E_i$ $(i = 1, 2, 3)$.

$\pi\Sigma N$ threshold. For instance, we have

$$S_{YN}^{\rm con}(E) \approx \text{const.} \times \frac{1}{D^2(E)} \tag{31}$$

for the $Y + N$ decay spectrum.

Now we consider the peak structure in the $[K^- pp] \to Y + N$ decay spectrum obtained with $V_0 = -292$ MeV and $W_0 = -107$ MeV for potential B. Figure 7 illustrates the pole trajectory $\omega(E)$ as a function of E, together with $D(E)$ and $1/D^2(E)$. When E is changed from 0 to -100 MeV, the pole moves slowly from the point (-42 MeV, -51 MeV) to the point (-51 MeV, -15 MeV), so that $D(E)$ works as an almost-smooth function with a minimum value at $E \simeq -60$ MeV. In this case, therefore, a clear peak in $1/D^2(E)$ is observed around $E \simeq -60$ MeV. This peak is in good agreement with that of the $Y + N$ decay spectrum in Fig. 5(b). The shape of the spectrum deviates from the standard BW form owing to the nature of the energy dependence of $D(E)$, whereas the position of this peak does not coincide with the point at $E = -$B.E. $= -45$ MeV.

Figure 5(c), on the contrary, shows a cusplike peak at the $\pi\Sigma N$ threshold in the $[K^- pp] \to Y + N$ decay spectrum with potential C. To understand the appearance of this cusplike structure, we obtain a moving pole at $\omega(E)$ with $V_0 = -344$ MeV and $W_0 = -203$ MeV for potential C, as a function of E. In Fig. 8 we illustrate the pole trajectory of its $\omega(E)$, $D(E)$, and $1/D^2(E)$. We find that the pole of $\omega(E)$ moves widely in the complex energy plane; when E is changed from 0 to -100 MeV, the pole of $\omega(E)$ moves from the point (-43 MeV, -110 MeV) to the point (-76 MeV, -34 MeV). For $E < E_{\rm th}(\pi\Sigma N)$, its pole remains around the point (-77 MeV, -25 MeV). It should be noted that the minimum of $D(E)$ is realized at $E = E_{\rm th}(\pi\Sigma N)$, where $dD(E)/dE$ is singular. In this case, therefore, a cusplike peak in $1/D^2(E)$ is observed at the $\pi\Sigma N$ threshold. This shape agrees with that of the spectrum shown in Fig. 5(c). To see the effects of W_0, we also obtain the trajectory of a moving pole with $V_0 = -344$ MeV and $W_0 = -47$ MeV, which corresponds to the specific case with an artificially

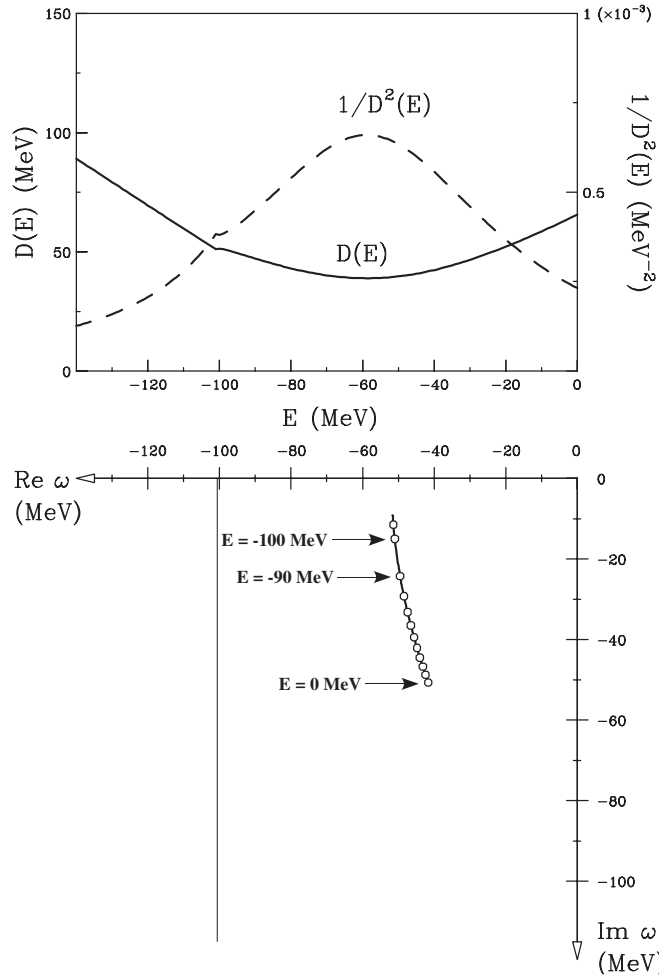

FIG. 7. Pole trajectory of the $K^- pp$ state (bottom) and $D(E)$ (top) in the complex energy plane, in the case of potential B ($V_0 = -292$ MeV and $W_0 = -107$ MeV). Circles denote pole positions at $\omega(E)$, which are drawn from $E = -110$ MeV to $E = 0$ MeV, in steps of 10 MeV. The dashed curve denotes $1/D^2(E)$, which roughly represents the contribution of the pole in the spectrum.

narrow width. We confirm that the shape of its spectrum is identified as the BW form, as shown in Fig. 9.

Consequently, we recognize that the cusplike structure can be described as the behavior of the pole trajectory, which is governed by the energy dependence of $U^{\rm opt}(E)$, as well as a clear peak with the BW form. The path of the trajectory for the moving pole in the complex energy plane is determined by the values of V_0, and its moving range on the trajectory depends on the values of W_0.

2. *Pole trajectories for K⁻-"pp" optical potentials*

Figure 10 shows the pole trajectories of the $K^- pp$ bound state for potentials A, B, C, D_1, D_2, and D_3 in the complex energy plane. The strength parameters (V_0, W_0) characterize the shape structure of the $K^- pp$ state in the spectrum with the $[K^- pp] \to Y + N$ decay from two-nucleon K^- absorption. For potential C, a cusp at the $\pi\Sigma N$ threshold appears clearly in the spectrum, as shown in Fig. 5(c), because the value of $D(E)$

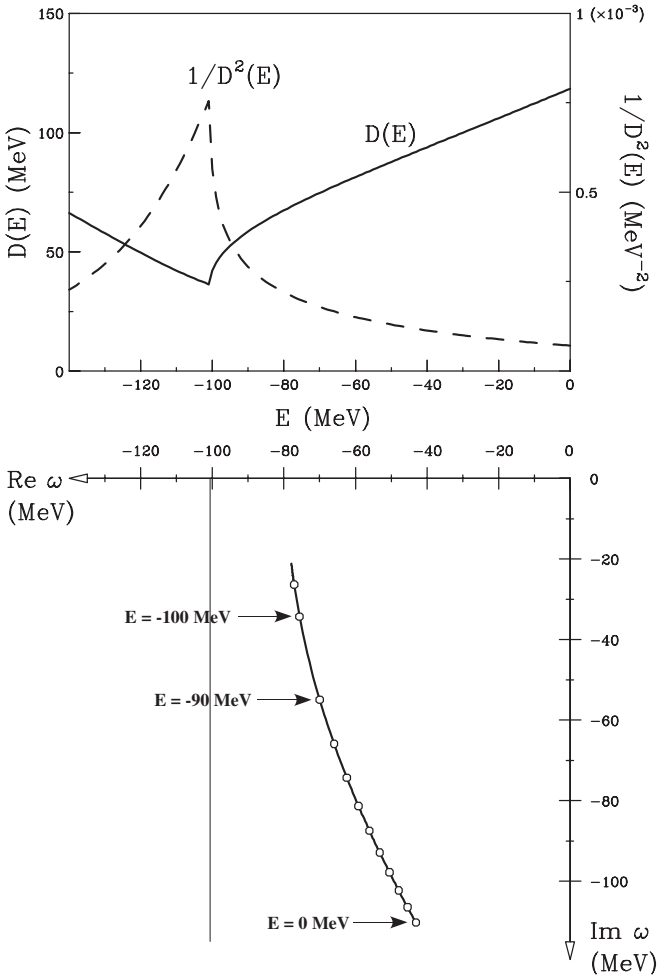

FIG. 8. Pole trajectory of the K^-pp state and $D(E)$ in the complex energy plane, in the case of potential C ($V_0 = -344$ MeV and $W_0 = -203$ MeV). See also the caption to Fig. 7.

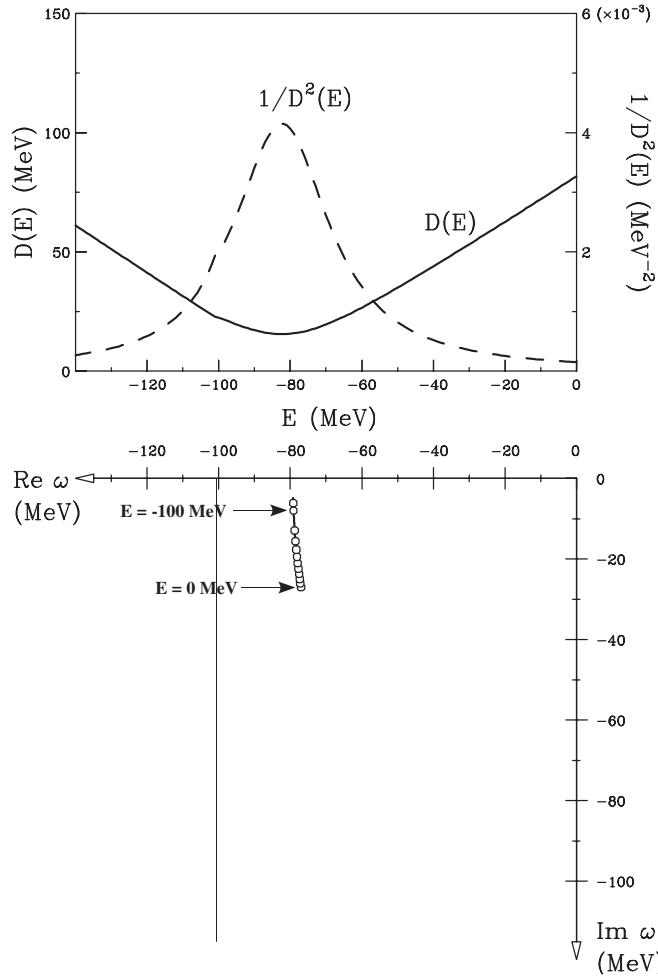

FIG. 9. Pole trajectory of the K^-pp state and $D(E)$ in the complex energy plane, in the case of potential C modified with an artificially narrow width ($V_0 = -344$ MeV and $W_0 = -47$ MeV). See also the caption to Fig. 7.

at $E = E_{\rm th}(\pi\Sigma N)$ is much smaller than that of $\Gamma/2$, which is equivalent to the distance from the pole at point $(-\text{B.E.}, -\Gamma/2)$ to the real axis. For potential D_2, a steep step is observed at the $\pi\Sigma N$ threshold, as shown in Fig. 5(d); its yield is sharply decreased because its pole moves rapidly above the $\pi\Sigma N$ threshold.

It should be noted that our K^--"pp" optical potentials, $U^{\rm opt}(E)$, are not derived from microscopic calculations but are introduced phenomenologically. To examine whether or not a potential has the appropriate energy dependence, we evaluate the pole trajectory of point $(-\text{B.E.}, -\Gamma/2)$ in the complex energy plane when we change the value of V_0 in $U^{\rm opt}(E)$.

Figure 11 shows the energy dependence of the pole trajectories on decay channels with $V_0 = (-300)$ to (-420) MeV, when we switch on/off each $B_1^{(\pi\Lambda N)}$ and $B_2^{(YN)}$, with $B_1^{(\pi\Sigma N)} = 0.7$ and $W_0 = -203$ MeV, which corresponds to the imaginary part of potential C. If we consider only $B_1^{(\pi\Sigma N)}$, its width becomes smaller when $-$B.E. is close to $E_{\rm th}(\pi\Sigma N)$, and it finally becomes 0 when $-$B.E. is located below $E_{\rm th}(\pi\Sigma N)$. This behavior seems to be qualitatively consistent with the result obtained from a $\bar{K}NN$-$\pi\Sigma N$ coupled-channel Faddeev calculation by Ikeda and Sato [43]. Even if $B_1^{(\pi\Lambda N)}$ and/or $B_2^{(YN)}$ is switched on, the pole trajectory of the point $(-\text{B.E.}, -\Gamma/2)$ is not much changed quantitatively, except for additional width. But the pole trajectory for the energy-independent potential $U_0^{\rm opt}$ differs from that for $U^{\rm opt}(E)$; $-\Gamma/2$ is almost proportional to $-$B.E. Therefore, we believe that our K^--"pp" optical potential $U^{\rm opt}(E)$ has the desirable energy dependence, which is expected from the coupled-channel Faddeev calculation, and that it is enough for us to discuss the shape of the spectrum with the $[K^-pp] \to Y + N$ decay process. For a more quantitative argument, one should obtain the $\bar{K}NN$ single-channel effective potential, in which the $\pi\Sigma N$ channel is eliminated in the $\bar{K}NN$-$\pi\Sigma N$ coupled-channel scheme [44], and compare it with our optical potential. Investigation along this line will be discussed in future work.

IV. DISCUSSION

A. Cusplike structure in the spectrum near the $\pi\Sigma N$ threshold

Recently, Akaishi *et al.* [45] discussed a cusplike structure in the spectrum of the (in-flight K^-,n) reaction on a deuteron

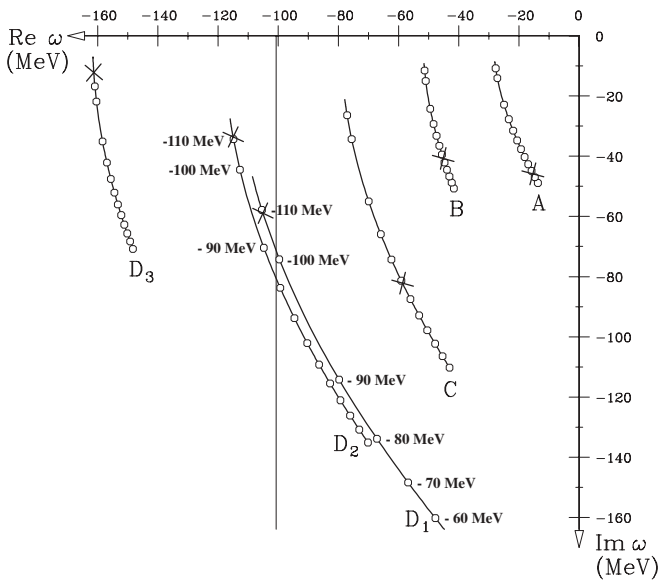

FIG. 10. Pole trajectories of the $K^- pp$ state for potentials A, B, C, D_1, D_2, and D_3 in the complex energy plane. Circles denote pole positions at $\omega(E)$, which are drawn from $E = -110$ MeV to $E = 0$ MeV, in steps of 10 MeV. Crosses denote positions at $(-\text{B.E.}, -\Gamma/2)$ whose values are given in Table I for these potentials.

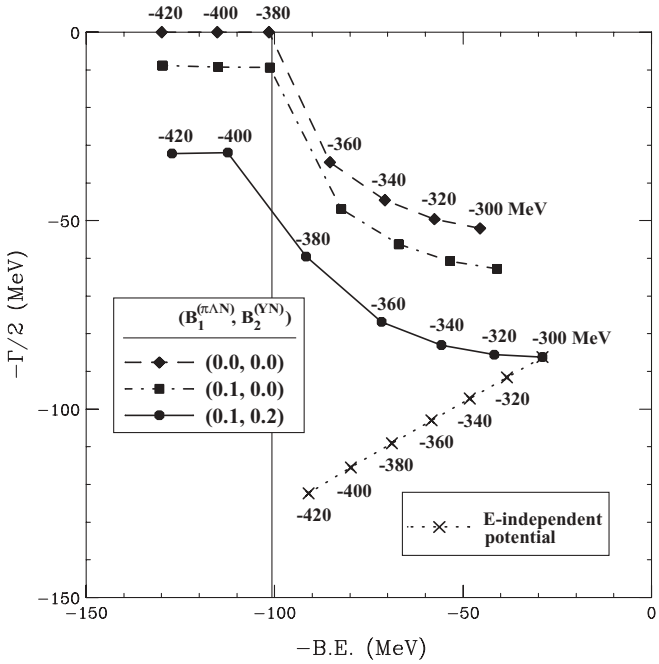

FIG. 11. Behavior of the moving pole at $(-\text{B.E.}, -\Gamma/2)$ when the value of V_0 for the energy-dependent potential $U^{\text{opt}}(E)$ is changed. Diamonds, squares, and circles denote the cases of $[B_1^{(\pi\Lambda N)}, B_2^{(YN)}] = (0.0, 0.0)$, $(0.1, 0.0)$, and $(0.1, 0.2)$ in $U^{\text{opt}}(E)$ with $B_1^{(\pi\Sigma N)} = 0.7$ and $W_0 = -203$ MeV, respectively. Crosses denote the case of the energy-independent potential U_0^{opt} with $W_0 = -179$ MeV. Numbers by the symbols give the corresponding values of V_0.

target, using a coupled-channel model with a separable potential. They showed that the cusplike structure at the $\pi\Sigma$ threshold can also be observed in the $[K^- p] \to \pi + \Sigma$ spectrum from one-nucleon K^- absorption. In Sec. III, we found a cusplike structure at the $\pi\Sigma N$ threshold in spectra with $[K^- pp] \to \pi + \Lambda + N$ and $[K^- pp] \to Y + N$ decay processes when using potential C. The shape and magnitude of these spectra depend strongly on the pole trajectory of the $K^- pp$ bound state and are characterized by the strength parameters (V_0, W_0). It is worth examining the conditions for (V_0, W_0) that gives the cusplike structure at the $\pi\Sigma N$ threshold within our optical potential $U^{\text{opt}}(E)$.

In this section, we focus on spectra with $[K^- pp] \to \pi + \Sigma + N$ and $[K^- pp] \to Y + N$ decays, by artificially changing (V_0, W_0) in the following two cases: (i) $[B_1^{(\pi\Sigma N)}, B_2^{(YN)}] = (0.7, 0.0)$, which means only the $[K^- pp] \to \pi + \Sigma + N$ decay process; and (ii) $[B_1^{(\pi\Sigma N)}, B_2^{(YN)}] = (0.7, 0.2)$. Here we omit $B_1^{(\pi\Lambda N)}$ for the $[K^- pp] \to \pi + \Lambda + N$ decay process for simplicity, because $B_1^{(\pi\Lambda N)}$ operates similarly to $B_2^{(YN)}$ in the spectrum, as discussed in Sec. III B.

Figure 12 shows the behaviors of $S(E)$ in spectra with $[K^- pp] \to \pi + \Sigma + N$ and $[K^- pp] \to Y + N$ decays at

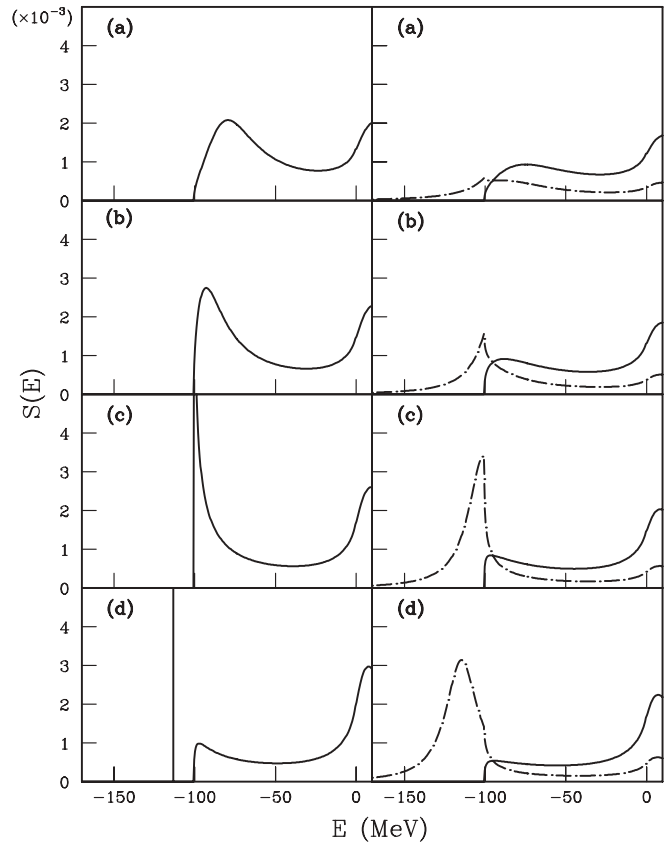

FIG. 12. Behavior of the strength function $S(E)$ at $W_0 = -107$ MeV when the value of V_0 is changed: $V_0 =$ (a) -340 MeV, (b) -360 MeV, (c) -380 MeV, and (d) -400 MeV in (left) the case of $[B_1^{(\pi\Sigma N)}, B_2^{(YN)}] = (0.7, 0.0)$ and (right) the case of $[B_1^{(\pi\Sigma N)}, B_2^{(YN)}] = (0.7, 0.2)$. Solid and dashed curves denote $S_{\pi\Sigma N}^{\text{con}}(E)$ and $S_{YN}^{\text{con}}(E)$, respectively.

$-W_0 = 107$ MeV, which corresponds to the imaginary part of potential B, by changing $-V_0 = 340$–400 MeV. For case (i), as shown in Fig. 12 (left), the magnitude of the peak in $S^{\rm con}_{\pi\Sigma N}(E)$ increases at the $\pi\Sigma N$ threshold with increasing $-V_0$. When $-V_0 \simeq 380$ MeV, the magnitude is at its maximum around $-$B.E. $\simeq E_{\rm th}(\pi\Sigma N)$. When $-V_0 > 380$ MeV, the $K^- pp$ state must be bound below the $\pi\Sigma N$ threshold and its peak is located at $E = -$B.E. This cusplike peak in $S^{\rm con}_{\pi\Sigma N}(E)$ is quite similar to that obtained by Akaishi *et al.* [45].

For case (ii), we show the behaviors of $S^{\rm con}_{YN}(E)$ and $S^{\rm con}_{\pi\Sigma N}(E)$ with $B_2^{(YN)} = 0.2$ in Fig. 12 (right). We find that there is a cusplike structure in $S^{\rm con}_{YN}(E)$ at $-V_0 \simeq 340$–380 MeV, and an asymmetric peak, which is cut off sharply above the $\pi\Sigma N$ threshold, appears in $S^{\rm con}_{YN}(E)$ when $-V_0 > 380$ MeV, whereas there is no (cusplike) peak in $S^{\rm con}_{\pi\Sigma N}(E)$. Thus, we recognize that the cusplike structure is observed in the $[K^- pp] \to Y + N$ decay spectrum rather than the $[K^- pp] \to \pi + \Sigma + N$ decay spectrum because of the existence of the $Y + N$ decay channel.

In Fig. 13, we examine the behaviors of $S(E)$ in spectra with $[K^- pp] \to \pi + \Sigma + N$ and $[K^- pp] \to Y + N$ decays at $-V_0 = 344$ MeV, which corresponds to the real part of potential C, by changing $-W_0 = 60$–200 MeV. In case (i), we see that the clear peak near $E \simeq -80$ MeV in $S^{\rm con}_{\pi\Sigma N}(E)$ becomes broad as $-W_0$ increases, as shown in Fig. 13 (left). In case (ii), we also find that a clear peak is located near $E \simeq -80$ MeV in both $S^{\rm con}_{\pi\Sigma N}(E)$ and $S^{\rm con}_{YN}(E)$ at $-W_0 = 60$ MeV, as shown in Fig. 13 (right). As $-W_0$ increases, $S^{\rm con}_{\pi\Sigma N}(E)$ gradually decreases, but $S^{\rm con}_{YN}(E)$ gradually increases just at the $\pi\Sigma N$ threshold. Thus it increases up to a threshold cusp in the spectrum.

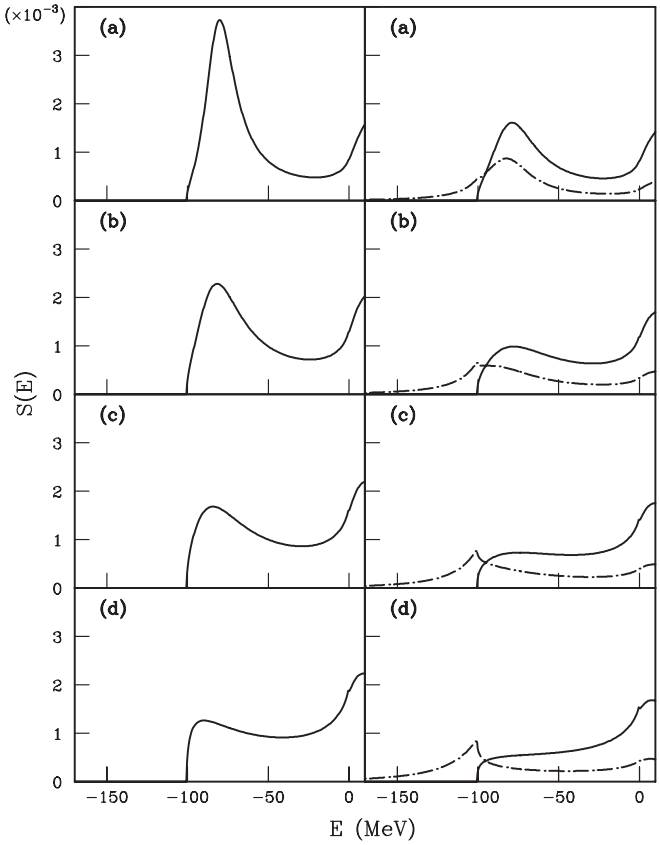

FIG. 13. Behavior of the strength function $S(E)$ at $V_0 = -344$ MeV when the value of W_0 is changed: $W_0 =$ (a) -60 MeV, (b) -100 MeV, (c) -140 MeV, and (d) -200 MeV. See also the caption to Fig. 12.

Therefore, we see the cusplike structure in the spectrum under the conditions that $-$B.E. is close to and above the $\pi\Sigma N$ threshold energy and Γ is very large. The corresponding strength parameters are roughly estimated as $-V_0 = 330$–380 MeV and $-W_0 \geqslant 100$–120 MeV, which are found for potential C, given in Table I. The cusplike structure is the unique signal for evidence of the deeply bound $K^- pp$ state in the $[K^- pp] \to Y + N$ decay spectrum.

B. Dependence of the spectrum on the branching rate $B_2^{(YN)}$

The shape of the semiexclusive K^- conversion spectrum including the $[K^- pp] \to Y + N$ decay process is very important for extracting the structure of the $K^- pp$ state, for example, the potential strengths (V_0, W_0), rather than that of the spectrum including the $[K^- pp] \to \pi + \Sigma + N$ decay process. In our calculations, we assumed the branching rate $B_2^{(YN)} = 0.2$ in $K^- pp$ decay processes. This value has often been used in previous work on heavier targets [26,27,41,42] but it is experimentally unknown for K^- absorption on ^{3}He in flight. In terms of K^- absorption on ^{4}He at rest, early data from a helium bubble chamber experiment [46] suggested that the ratio of two-nucleon K^- absorption to all K^- absorption processes amounts to 16%, whereas its value depends on atomic orbits where K^- is absorbed through atomic cascade processes [27,47]. A recent analysis of K^- absorption on ^{4}He at rest [48] also calls for re-examination of $B_2^{(YN)}$ experimentally. To determine the value of $B_2^{(YN)}$ in K^- absorption in flight, we need more investigations on $B_2^{(YN)}$, experimentally and theoretically.

As the first step toward these investigations, we attempted to calculate the strength function $S(E)$ for potential C, to check the sensitivity of semiexclusive spectra to the value of $B_2^{(YN)}$. Figure 14 demonstrates the dependence of the spectra on the values of $B_2^{(YN)}$ when changing $B_2^{(YN)} = 0.1$–0.3. For the $[K^- pp] \to \pi + \Sigma + N$ and $[K^- pp] \to \pi + \Lambda + N$ decay spectra, each magnitude is reduced as $B_2^{(YN)}$ increases, as shown in Figs. 14(a) and 14(b). On the contrary, the $[K^- pp] \to Y + N$ decay spectrum is enhanced as $B_2^{(YN)}$ increases, as shown in Fig. 14(c). The shape of these spectra is scarcely modified by a small change in $B_2^{(YN)}$. Thus, the detailed values of the branching rates have an influence only on the relative magnitude of each decay spectrum, and do not change the nature of the $K^- pp$ formation signal. We stress that it is important to compare the shapes of calculated spectra with those of measured spectra. This detailed comparison provides valuable information on $B_2^{(\pi\Sigma N)}$, $B_2^{(\pi\Lambda N)}$, and $B_2^{(YN)}$, as well as on the binding energy and width of the $K^- pp$ state.

C. The spectrum near the $K^- + p + p$ threshold

Figure 5(a) shows the partial contributions in the spectra with potential A. The spectra have no clear peak because

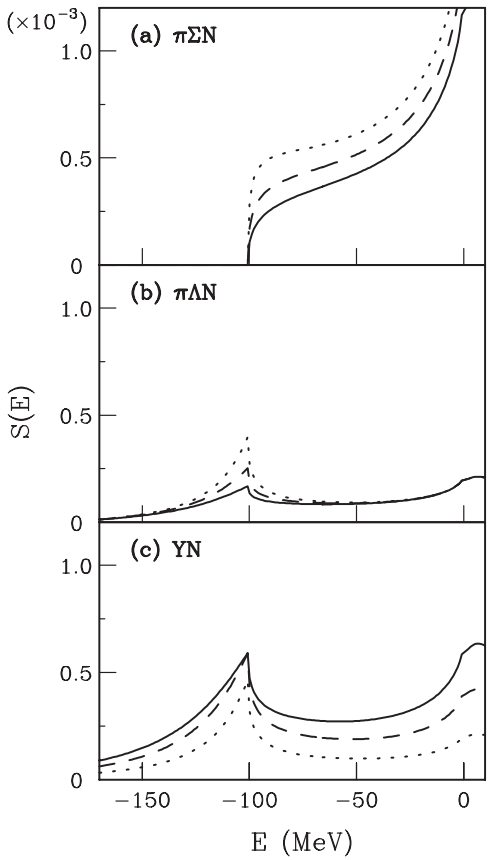

FIG. 14. Behavior of the calculated strength functions $S(E)$ for (a) $[K^- pp] \to \pi + \Sigma + N$, (b) $[K^- pp] \to \pi + \Lambda + N$, and (c) $[K^- pp] \to Y + N$ decay processes. Here potential C with $B_1^{(\pi\Lambda N)} = 0.1$ is used. Dotted, dashed, and solid curves denote the spectra for $[B_1^{(\pi\Sigma N)}, B_2^{(YN)}] = (0.8, 0.1)$, (0.7, 0.2), and (0.6, 0.3), respectively.

the pole for potential A has a large width and is located near the $K^- + p + p$ threshold. To extract information on the K^--"pp" potential from the spectral shapes, one must consider the effect of the $K^- + p + p$ threshold beyond the "pp" core assumption. If "pp" $\to p + p$ degrees of freedom is taken into account, a QF $\Lambda(1405)$ formation via $[K^- pp] \to$ "$K^- p$" $+ p \to \Lambda(1405) + p$ would be important, rather than $[K^- pp] \to K^- + p + p$ breakup processes. The spectrum of such a QF $\Lambda(1405)$ formation stands up from $E \simeq (-10)$ to (-20) MeV below the $K^- + p + p$ threshold, which depends on the $\Lambda(1405)$ mass as a $\bar{K}$-N quasibound state. In the case of B.E. $\simeq 20$ MeV obtained for potential A, therefore, it may be necessary to estimate the contribution of the QF $\Lambda(1405)$ spectrum, which contaminates the $K^- pp$ formation spectrum near the $K^- + p + p$ threshold.

V. SUMMARY AND CONCLUSION

We have examined inclusive and semiexclusive spectra in the ^{3}He(in-flight K^-,n) reaction at $p_{K^-} = 1.0\,\mathrm{GeV}/c$ and $\theta_{\mathrm{lab}} = 0^\circ$ for the forthcoming J-PARC E15 experiment. We have discussed these spectra with energy-dependent K^--"pp" optical potentials $U^{\mathrm{opt}}(E)$, based on the results for binding energies and widths of $K^- pp$ (unstable) bound states in several predictions or candidates. To understand the peak structure in the spectrum, we have investigated the trajectory of a moving pole of the $K^- pp$ bound state in the complex energy plane and the behavior of the corresponding strength function by changing the strength parameters (V_0, W_0) of $U^{\mathrm{opt}}(E)$ systematically. The calculated spectrum predominantly has a bound state with $I = 1/2$, $J^\pi = 0^-$, and $L = 0$ in the $K^- pp$ bound region below the $K^- + p + p$ threshold, whereas continuum states with $L \geqslant 1$ occur in the QF region. We have shown that the (in-flight K^-,n) reaction on s-shell nuclear targets such as ^{3}He provides the advantage of producing a deeply bound K^- nuclear state with $L = 0$. The results can be summarized as follows:

(i) A clear peak appears below the $\pi\Sigma N$ threshold in the spectrum with $[K^- pp] \to Y + N$ decay from two-nucleon K^- absorption as evidence of the $K^- pp$ bound state, within $-V_0 > 380$ MeV, as in the case of potential D.

(ii) A cusplike structure appears at the $\pi\Sigma N$threshold in the $[K^- pp] \to Y + N$ decay spectrum within $-V_0 \simeq$ 330–380 MeV and $-W_0 > \sim$110 MeV, rather than in the $[K^- pp] \to \pi + \Sigma + N$ decay spectrum, as in the case of potential C.

(iii) A distinct peak in the $[K^- pp] \to Y + N$ and $[K^- pp] \to \pi + \Sigma + N$ decay spectra is observed as clear evidence of the $K^- pp$ bound state within $-V_0 \simeq$ 200–330 MeV and $-W_0 < \sim$110 MeV, such as for potential B, whereas no clear peak is observed in these spectra even if the $K^- pp$ bound state exists within $-V_0 \simeq$ 200–330 MeV and $-W_0 > \sim$110 MeV, such as for potential A.

In conclusion, the ^{3}He(in-flight K^-,n) spectrum including the $[K^- pp] \to Y + N$ decay process from two-nucleon K^- absorption provides evidence of the $K^- pp$ bound state to identify itself as the appropriate K^--"pp" potential with the help of the trajectory of its moving pole in the complex energy plane. If any of the experimental observations of DISTO [18], FINUDA [15], and OBELIX [17] indicate evidence of the $K^- pp$ bound state, its corresponding peak should appear below the $\pi\Sigma N$ threshold in the J-PARC E15 spectrum. Otherwise, all these experimental data may be incorrect. Moreover, a cusplike structure is the unique signal of the $K^- pp$ formation, as well as the peak structure. This phenomenology suggests the possibility of observing a cusplike structure obtained by a deep potential with strong absorption ($-V_0 = 330$–380 MeV, $-W_0 > 110$ MeV), as predicted by Shevchenko *et al.* [5]. If a cusplike structure is observed, a precise comparison between theoretical and experimental spectra is required to extract the binding energy and width of the $K^- pp$ state, as well as analysis of the spectrum in which the clear peak is observed. To obtain more quantitative results on the cusplike or peak structure, a full microscopic calculation between $\bar{K}NN$ and πYN channels would be required beyond our optical potential models. Nevertheless, we believe that our calculations lead to good insight for qualitative understanding of the spectrum of the deeply bound $K^- pp$ state.

ACKNOWLEDGMENTS

We acknowledge Professor M. Iwasaki, Dr. H. Ohta, Dr. H. Ohnishi, and Dr. T. Suzuki for discussions of the plan for the J-PARC E15 experiment. We thank Professor Y. Akaishi for many valuable discussions and suggestions. This work was supported by Grants-in-Aid for Scientific Research in Priority Areas (Nos. 17070002, 17070007, and 20028012).

[1] D. B. Kaplan and A. E. Nelson, Phys. Lett. **B175**, 57 (1986); G. E. Brown and M. Rho, Phys. Rep. **269**, 333 (1996); C. H. Lee, *ibid.* **275**, 255 (1996).
[2] A. Doté, H. Horiuchi, Y. Akaishi, and T. Yamazaki, Phys. Rev. C **70**, 044313 (2004).
[3] Y. Nogami, Phys. Lett. **7**, 288 (1963).
[4] T. Yamazaki and Y. Akaishi, Phys. Lett. **B535**, 70 (2002); Proc. Jpn. Acad. Ser. B **83**, 144 (2007); arXiv:0805.4382 [nucl-th].
[5] N. V. Shevchenko, A. Gal, and J. Mareš, Phys. Rev. Lett. **98**, 082301 (2007); N. V. Shevchenko, A. Gal, J. Mareš, and J. Revai, Phys. Rev. C **76**, 044004 (2007).
[6] Y. Ikeda and T. Sato, Phys. Rev. C **76**, 035203 (2007).
[7] A. Doté, T. Hyodo, and W. Weise, Nucl. Phys. **A804**, 197 (2008); Phys. Rev. C **79**, 014003 (2009).
[8] A. N. Ivanov, P. Kienle, J. Marton, and E. Widmann, nucl-th/0512037.
[9] T. Nishikawa and Y. Kondo, Phys. Rev. C **77**, 055202 (2008).
[10] A. Arai, M. Oka, and S. Yasui, Prog. Theor. Phys. **119**, 103 (2008).
[11] J. Yamagata, D. Jido, H. Nagahiro, and S. Hirenzaki, Mod. Phys. Lett. A **23**, 2528 (2008); J. Yamagata-Sekihara, D. Jido, H. Nagahiro, and S. Hirenzaki, Phys. Rev. C **80**, 045204 (2009).
[12] S. Wycech and A. M. Green, Phys. Rev. C **79**, 014001 (2009).
[13] E. Oset and A. Ramos, Nucl. Phys. **A635**, 99 (1998); E. Oset, A. Ramos, and C. Bennhold, Phys. Lett. **B527**, 99 (2002).
[14] T. Hyodo and W. Weise, Phys. Rev. C **77**, 035204 (2008).
[15] M. Agnello *et al.*, Phys. Rev. Lett. **94**, 212303 (2005).
[16] V. K. Magas, E. Oset, A. Ramos, and H. Toki, Phys. Rev. C **74**, 025206 (2006).
[17] G. Bendiscioli *et al.*, Nucl. Phys. **A789**, 222 (2007).
[18] T. Yamazaki *et al.*, Hyperfine Interact. **193**, 181 (2009).
[19] M. Iwasaki *et al.*, J-PARC proposal, http://j-parc.jp/NuclPart/pac_0606/pdf/p15-Iwasaki.pdf.
[20] K. Suzuki *et al.*, Hyperfine Interact. **193**, 189 (2009).
[21] T. Yamazaki and Y. Akaishi, Phys. Rev. C **76**, 045201 (2007).
[22] P. Kienle, Nucl. Phys. **A804**, 286 (2008).
[23] T. Koike and T. Harada, Phys. Lett. **B652**, 262 (2007).
[24] O. Morimatsu and K. Yazaki, Nucl. Phys. **A483**, 493 (1988); Prog. Part. Nucl. Phys. **33**, 679 (1994).
[25] T. Harada, Phys. Rev. Lett. **81**, 5287 (1998); Nucl. Phys. **A672**, 181 (2000); T. Harada and Y. Hirabayashi, *ibid.* **A759**, 143 (2005).
[26] T. Kishimoto *et al.*, Prog. Theor. Phys. **118**, 181 (2007).
[27] J. Yamagata, H. Nagahiro, and S. Hirenzaki, Phys. Rev. C **74**, 014604 (2006); J. Yamagata and S. Hirenzaki, Eur. Phys. J. A **31**, 255 (2007).
[28] T. Koike and T. Harada, Nucl. Phys. **A804**, 231 (2008).
[29] K. Ikuta, M. Arima, and K. Masutani, Prog. Theor. Phys. **108**, 917 (2002).
[30] T. Koike and T. Harada, Mod. Phys. Lett. A **23**, 2540 (2008); **24**, 911 (2009); Int. J. Mod. Phys. A **24**, 2126 (2009); Hyperfine Interact. **193**, 221 (2009).
[31] J. Hüfner, S. Y. Lee, and H. A. Weidenmüller, Nucl. Phys. **A234**, 429 (1974).
[32] S. Tadokoro, H. Kobayashi, and Y. Akaishi, Phys. Rev. C **51**, 2656 (1995).
[33] T. Kishimoto, Phys. Rev. Lett. **83**, 4701 (1999).
[34] G. P. Gopal *et al.*, Nucl. Phys. **B119**, 362 (1977).
[35] A. S. Rosenthal and F. Tabakin, Phys. Rev. C **22**, 711 (1980).
[36] C. B. Dover and A. Gal, Ann. Phys. (NY) **146**, 309 (1983).
[37] I. Angeli, At. Data Nucl. Data Tables **87**, 185 (2004).
[38] Particle Data Group, C. Amsler *et al.*, Phys. Lett. **B667**, 1 (2008).
[39] A. Cieplý, E. Friedman, A. Gal, and J. Mareš, Nucl. Phys. **A696**, 173 (2001).
[40] C. B. Dover, L. Ludeking, and G. E. Walker, Phys. Rev. C **22**, 2073 (1980).
[41] J. Mareš, E. Friedman, and A. Gal, Phys. Lett. **B606**, 295 (2005); Nucl. Phys. **A770**, 84 (2006).
[42] D. Gazda, E. Friedman, A. Gal, and J. Mareš, Phys. Rev. C **76**, 055204 (2007); J. Mareš, Nucl. Phys. **A804**, 296 (2008).
[43] Y. Ikeda and T. Sato, Phys. Rev. C **79**, 035201 (2009).
[44] H. Feshbach, Ann. Phys. (NY) **5**, 357 (1958); **19**, 287 (1962).
[45] Y. Akaishi, Khin Swe Myint, and T. Yamazaki, Proc. Jpn. Acad. Ser. B **84**, 264 (2008); arXiv:0805.4382 [nucl-th].
[46] P. A. Katz, K. Bunnel, M. Derrik, T. Fields, L. G. Hyman, and G. Keys, Phys. Rev. D **1**, 1267 (1970).
[47] T. Onaga, H. Narumi, and T. Kouhmura, Prog. Theor. Phys. **82**, 222 (1989).
[48] T. Suzuki *et al.*, Mod. Phys. Lett. A **23**, 2520 (2008); Phys. Rev. C **76**, 068202 (2007).